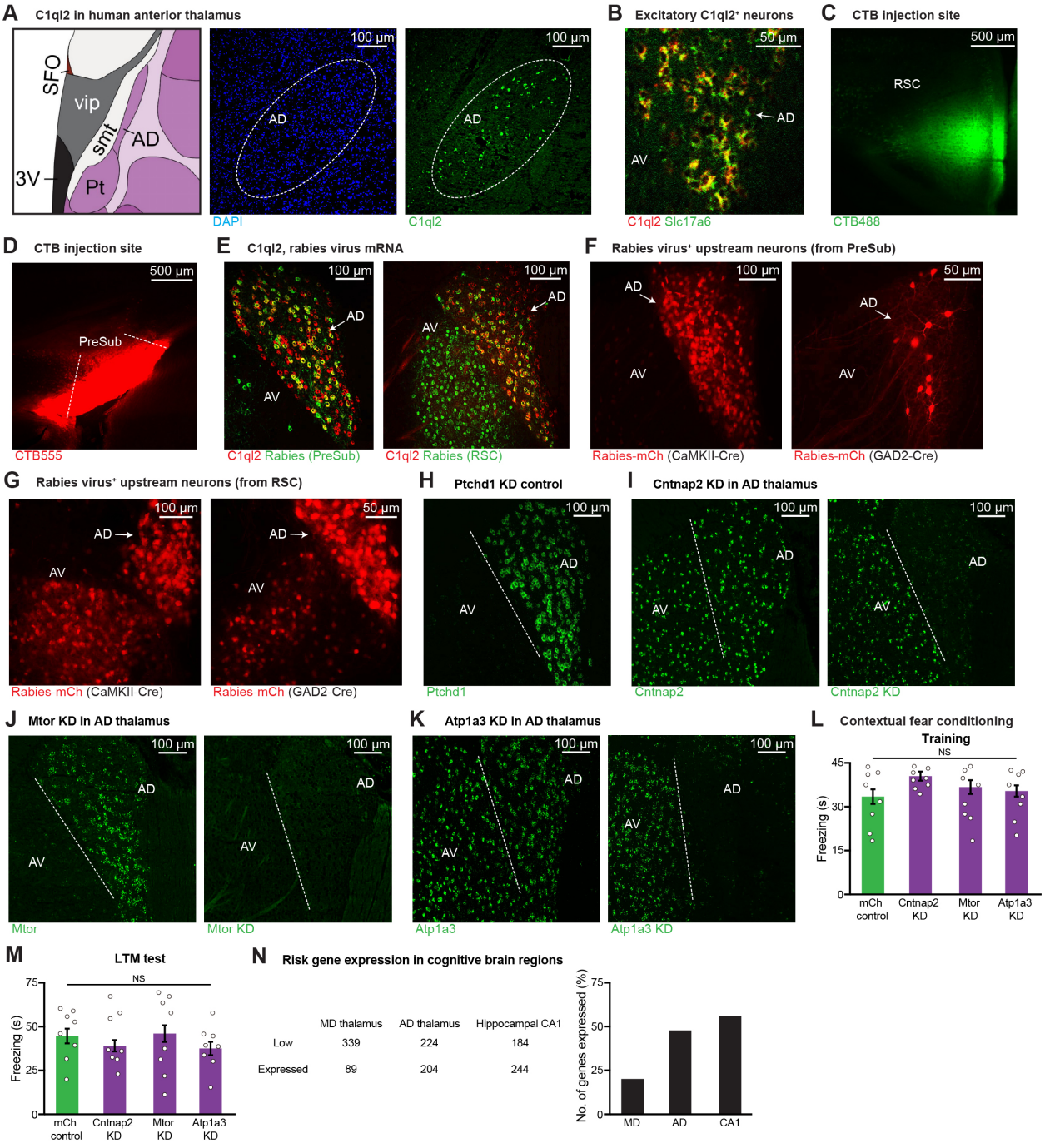

Figure S1. *C1QL2* Expression in Human ATN, AD/AV Outputs, and Risk Gene KD in AD, Related to Figures 1 and 2

(A) *C1ql2* FISH staining in human anterior thalamus tissue. Reference atlas image from the Allen Institute showing human AD, DAPI staining (blue), and *C1ql2* staining (green).

(B) *C1ql2*, *Slc17a6* FISH staining in mouse AD. Over 95% of all *Slc17a6*$^{+}$ neurons in AD expressed *C1ql2* (n = 3 mice). *Slc17a6* is also known as *Vglut2*, a marker of excitatory neurons.

(C-D) RSC (C) and PreSub (D) CTB injection sites.

(E) Retrograde rabies virus (RV), which was injected into PreSub or RSC, and *C1ql2* FISH staining in mouse ATN. Over 89% of all PreSub-projecting RV^+ neurons were $C1ql2^+$, and over 92% of all RSC-projecting RV^+ neurons were $C1ql2^+$ (n = 3 mice per group).

(F-G) Retrograde tracing using excitatory CaMKII-Cre and inhibitory GAD2-Cre mice by injecting Cre-dependent RV into PreSub or RSC. AD/AV retrograde labeling from PreSub (F) or RSC (G). An average of 192 RV^+ and 14 RV^+ cells were observed in AD from $CaMKII^+$ and $GAD2^+$ PreSub cells, respectively (n = 3 mice). An average of 152 RV^+ and 114 RV^+ cells were observed in AD from $CaMKII^+$ and $GAD2^+$ RSC cells, respectively (n = 3 mice).

(H) *Ptchd1* FISH staining in a mCh control virus injected mouse, which is related to the *in vivo* KD experiments.

(I-K) Using the circuit-based approach described in Figure 1H, *CNTNAP2* KD (I), *MTOR* KD (J), and *ATP1A3* KD (K) was performed in AD neurons, as revealed by FISH staining. *Cntnap2*, *Mtor*, and *Atp1a3* expression is decreased by 94%, 98%, and 96% (fluorescence intensity) respectively in KD mice as compared to mCh control mice (n = 3 mice per group).

(L-M) CFC training (L) and LTM recall tests (M) in *CNTNAP2*, *MTOR*, and *ATP1A3* KD mice (n = 8 mice per group).

(N) ASD and schizophrenia risk gene expression in mediodorsal (MD) thalamus, AD thalamus, and hippocampal CA1. Counts are based on 428 ASD and schizophrenia risk genes. Plot shows risk gene counts that are clearly expressed in each of these brain regions.

One-way ANOVA followed by Bonferroni post-hoc test (L-M). NS, not significant.

Data are presented as mean ± SEM.

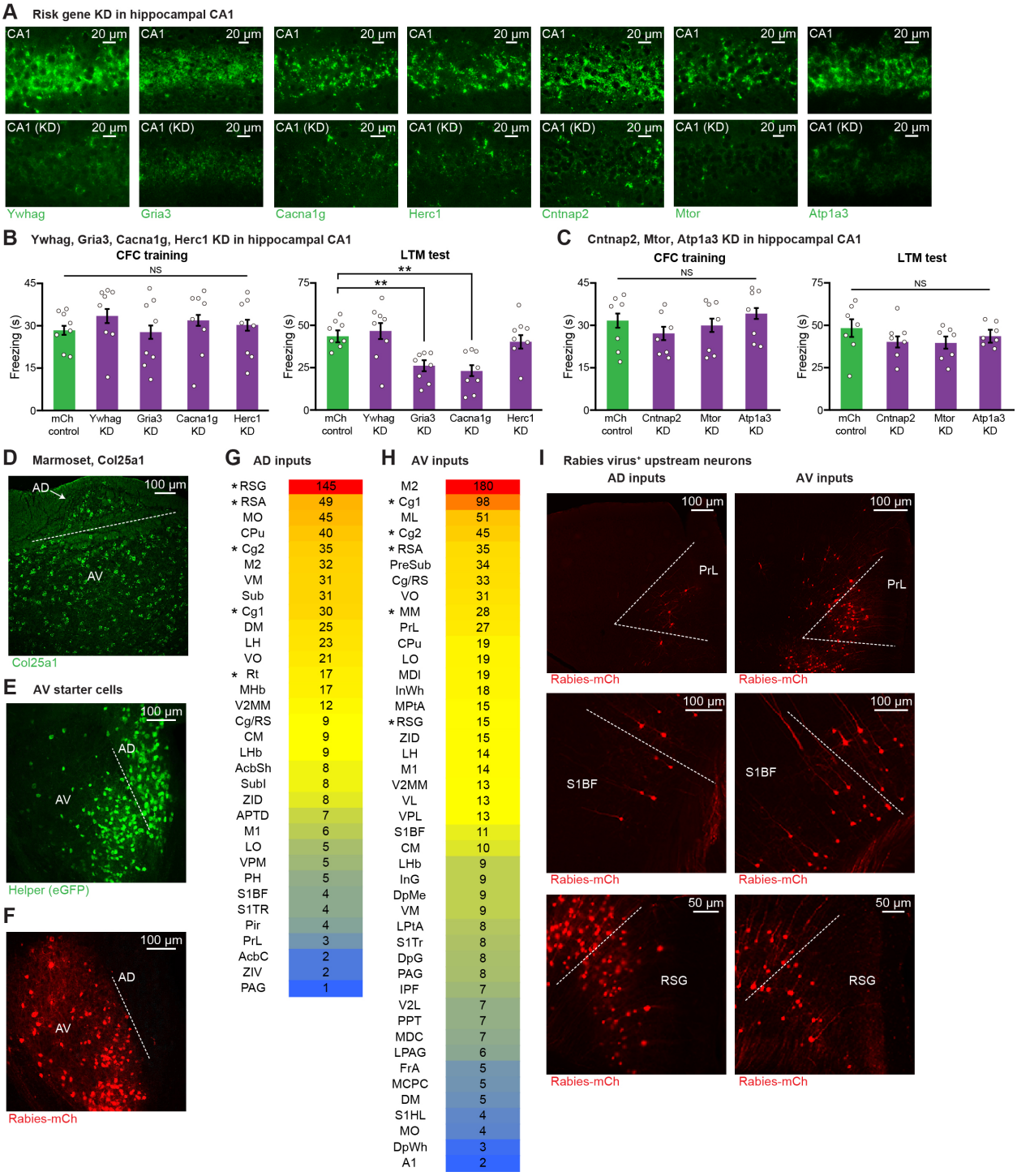

Figure S2. Risk Gene KD in Hippocampal CA1, *COL25A1* Expression in Marmosets, and Brain-Wide Input Patterns of AD/AV Thalamus, Related to Figures 2 and 3

(A) FISH staining demonstrates successful KD of various risk genes from hippocampal CA1 using a virus cocktail expressing target guide RNAs and constitutive SpCas9. In the control group (referred to as mCh control), a mCherry virus replaced the guide RNA virus and the SpCas9 virus was identical. The top row shows staining in mCh control tissue, whereas the

bottom row shows staining in individual KD mice. *Ywhag*, *Gria3*, *Cacna1g*, *Herc1*, *Cntnap2*, *Mtor*, and *Atp1a3* expression is decreased by 90%, 88%, 91%, 89%, 88%, 94%, and 95% (fluorescence intensity) respectively in KD mice as compared to mCh control mice (n = 3 mice per group).

(B) KD of *YWHAG*, *GRIA3*, *CACNA1G*, and *HERC1* from CA1 followed by CFC training and LTM recall tests (n = 8 mice per group). The KD of these four genes individually from AD neurons led to CFC deficits.

(C) KD of *CNTNAP2*, *MTOR*, and *ATP1A3* from CA1 followed by CFC training and LTM recall tests (n = 7 mice per group). The KD of these three genes individually from AD neurons did not alter CFC memory behavior.

(D) FISH staining in marmoset ATN showing *Col25a1* expression. Dashed line indicates the border between AD and AV.

(E-F) Individual helper (GFP, green) (E) and RV (mCherry, red) (F) channels showing restriction of RV labeling (i.e., starter cells) to mouse AV thalamus. Dashed line indicates the border between AD and AV. Surgery information is provided in the legend of Figure 3C.

(G-H) Inputs to AD (G) or AV (H) rank-ordered from highest to lowest average RV-positive cell counts (n = 3 mice for AD, n = 4 mice for AV, normalized starter cells across groups). Regions with an asterisk are among those reported in the literature previously (Jankowski et al., 2013).

A1 (primary auditory cortex), AcbC (accumbens nucleus core), AcbSh (accumbens nucleus shell), APTD (anterior pretectal nucleus dorsal part), Cg1 (cingulate cortex area 1), Cg2 (cingulate cortex area 2), Cg/RS (cingulate retrosplenial), CM (central medial thalamic nucleus), CPu (caudate putamen, dorsal striatum), DM (dorsomedial hypothalamic nucleus), DpG (deep gray layer of the superior colliculus), DpMe (deep mesencephalic nucleus), DpWh (deep white layer of the superior colliculus), FrA (frontal association cortex), InG (intermediate gray layer of the superior colliculus), InWh (intermediate white layer of the superior colliculus), IPF (interpeduncular fossa), LH (lateral hypothalamic area), LHb (lateral habenular nucleus), LO (lateral orbital cortex), LPAG (lateral periaqueductal gray), LPtA (lateral parietal association cortex), M1 (primary motor cortex), M2 (secondary motor cortex), MCPC (magnocellular nucleus of the posterior commissure), MDc (mediodorsal thalamic nucleus central part), MDl (mediodorsal thalamic nucleus lateral part), MHb (medial habenular nucleus), ML (medial mammillary nucleus, lateral part), MM (medial mammillary nucleus, medial part), MO (medial orbital cortex), MPtA (medial parietal association cortex), PAG (periaqueductal gray), PH (posterior hypothalamic area), Pir (piriform cortex), PPT (posterior pretectal nucleus), PrL (prelimbic cortex), RSA (retrosplenial agranular cortex), RSG (retrosplenial granular cortex), Rt (reticular thalamic nucleus), S1BF (primary somatosensory cortex barrel field), S1HL (primary somatosensory cortex hindlimb region), S1TR (primary somatosensory cortex trunk region), Sub (submedius thalamic nucleus), SubI (subincertal nucleus), V2L (secondary visual cortex lateral area), V2MM (secondary visual cortex mediomedial area), VL (ventrolateral thalamic nucleus), VM (ventromedial thalamic nucleus), VO (ventral orbital cortex), VPM (ventral posteromedial thalamic nucleus), VPL (ventral posterolateral thalamic nucleus), ZID (zona incerta dorsal part), ZIV (zona incerta ventral part).

(I) RV labeling in AD or AV tracing mice showing PrL, S1BF, and RSG brain regions.

One-way ANOVA followed by Bonferroni post-hoc test (B-C). For statistical comparisons, **p < 0.01; NS, not significant.

Data are presented as mean ± SEM.

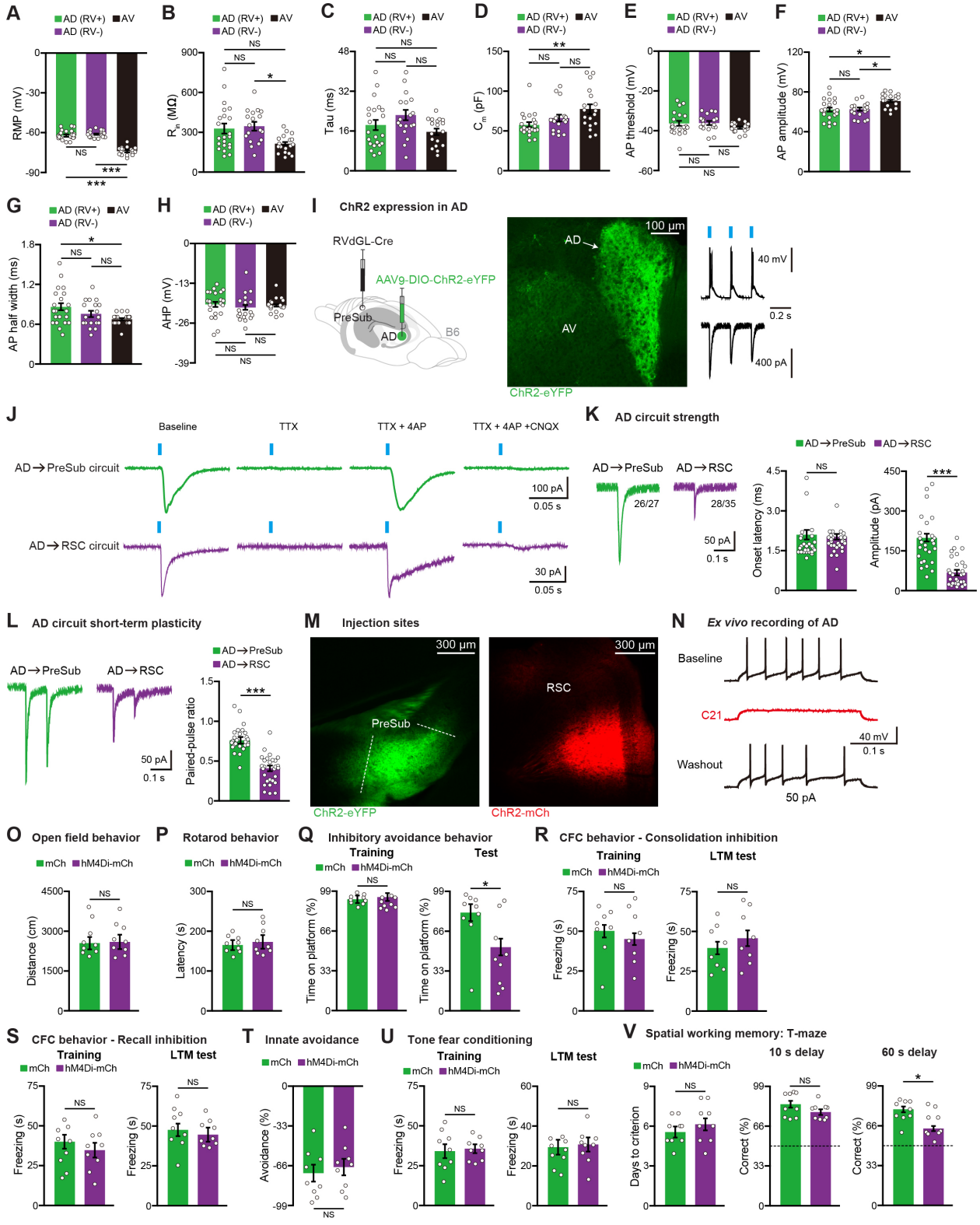
A
AD (RV+) AV
AD (RV-)
RMP (mV)
B
R_n (MΩ)
C
Tau (ms)
D
C_m (pF)
E
AP threshold (mV)
F
AP amplitude (mV)
G
AP half width (ms)
H
AHP (mV)
I
ChR2 expression in AD
RVdGL-Cre
AAV9-DIO-ChR2-eYFP
PreSub
AD
B6
100 µm
AV
40 mV
0.2 s
400 pA
ChR2-eYFP
J
Baseline
TTX
TTX + 4AP
TTX + 4AP +CNQX
AD→PreSub circuit
AD→RSC circuit
100 pA
0.05 s
30 pA
K
AD circuit strength
AD→PreSub
AD→RSC
26/27
28/35
50 pA
0.1 s
Onset latency (ms)
Amplitude (pA)
L
AD circuit short-term plasticity
Paired-pulse ratio
M
Injection sites
300 µm
RSC
ChR2-eYFP
ChR2-mCh
N
Ex vivo recording of AD
Baseline
C21
Washout
40 mV
0.1 s
50 pA
O
Open field behavior
mCh hM4Di-mCh
Distance (cm)
P
Rotarod behavior
Latency (s)
Q
Inhibitory avoidance behavior
Training
Test
Time on platform (%)
R
CFC behavior - Consolidation inhibition
LTM test
Freezing (s)
S
CFC behavior - Recall inhibition
T
Innate avoidance
Avoidance (%)
U
Tone fear conditioning
V
Spatial working memory: T-maze
10 s delay
60 s delay
Days to criterion
Correct (%)
NS
*
**
***

Figure S3. Electrophysiological Properties of AD/AV Neurons and AD Circuits, and Role of AD Thalamus in Various Behavioral Paradigms, Related to Figures 3 and 4

(A-H) Resting membrane potential or RMP (A), input resistance or R_{in} (B), membrane time constant or tau (C), membrane capacitance or C_m (D), action potential (AP) threshold (E), AP amplitude (F), AP half width (G), after-hyperpolarization potential (AHP) (H) (22 AD RV^+, 17 AD RV^-, 18 AV neurons, n = 3 mice). Surgery information is provided in the legend of Figure 3F.

(I) Channelrhodopsin-2 (ChR2) expression in mouse AD by injecting a retrograde RV expressing Cre into PreSub and Cre-dependent ChR2-eYFP in AD, current clamp (right top) or voltage clamp (right bottom) traces show light responses.

(J) Demonstration of monosynaptic connectivity in *ex vivo* optogenetic mouse brain slice recordings from AD circuits. TTX (tetrodotoxin), 4AP (4 aminopyridine), CNQX (cyanquixaline).

(K-L) Light-induced current traces, onset latency, amplitude of AD circuits (K), traces, paired-pulse ratio of AD circuits (L) (26/27 AD→PreSub and 28/35 AD→RSC neurons had responses, n = 3 mice).

(M) Anterograde labeling experiments, PreSub and RSC injection sites.

(N) C21-induced AD neuronal inhibition *ex vivo* using a 50 pA step current injection protocol.

(O-V) C21 was injected prior to the open field test session (15 min duration) (O), rotarod test (3 trials) (P), and inhibitory avoidance training, which was followed by a recall test 24 hr later (Q) (n = 9 mice per group). C21 was injected immediately after CFC training to inhibit AD during the cellular consolidation phase followed by a LTM test 24 hr later (R) (n = 8 mice per group). C21 was injected prior to the CFC LTM recall test (S), innate avoidance test (T), tone fear conditioning training, which was followed by a recall test 24 hr later (U), and prior to the T-maze spatial working memory training, 10 s delay tests, and 60 s delay tests (V) (n = 9 mice per group). mCherry control (mCh). Surgery information is provided in the legend of Figure 4A.

One-way ANOVA followed by Bonferroni post-hoc test (A-H), and two-tailed unpaired t test (K-L, O-V). For statistical comparisons, *$p < 0.05$, **$p < 0.01$, ***$p< 0.001$; NS, not significant.

Data are presented as mean ± SEM.

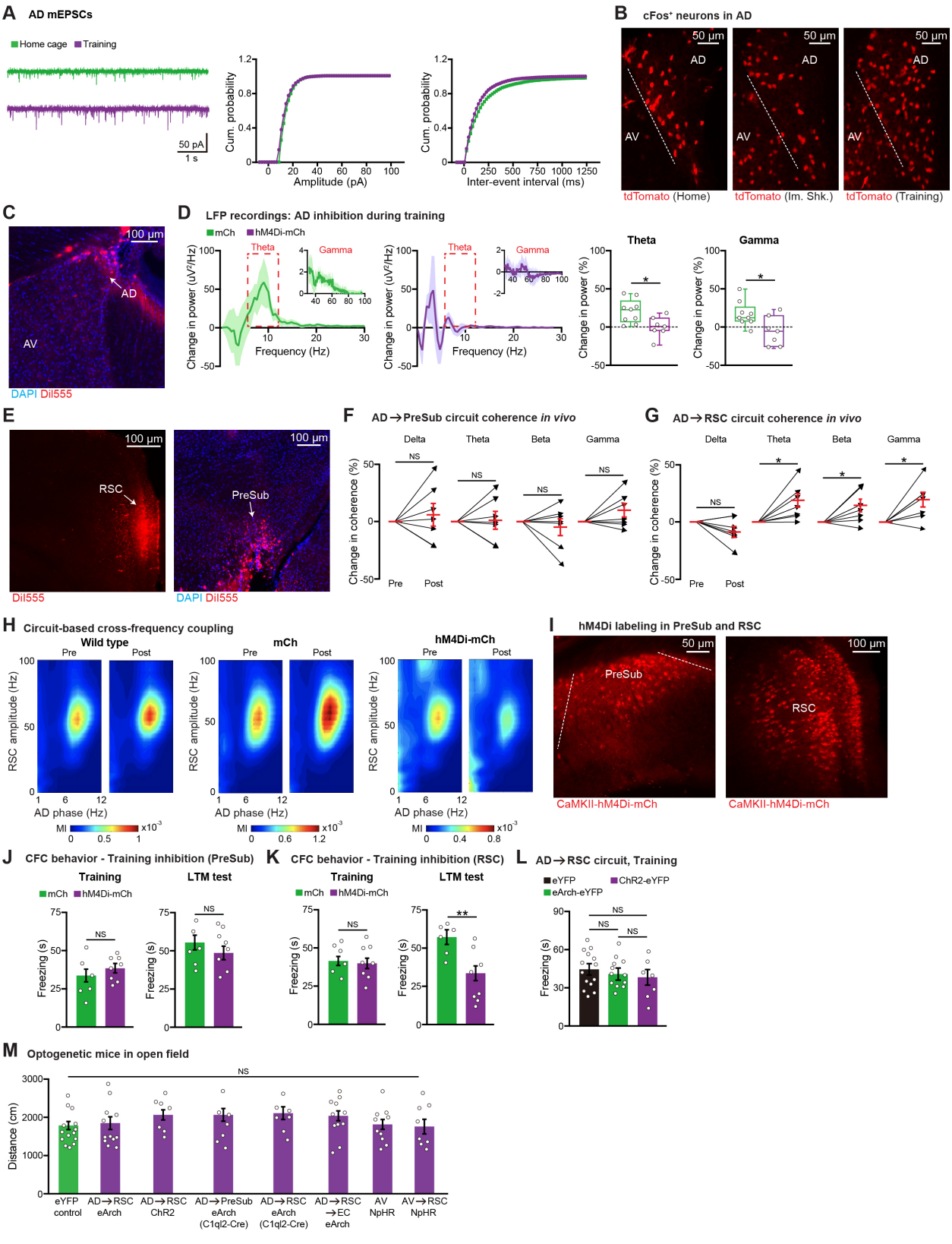
A
AD mEPSCs
Home cage
Training
50 pA
1 s
Cum. probability
Amplitude (pA)
Inter-event interval (ms)
B
cFos+ neurons in AD
50 μm
AD
AV
tdTomato (Home)
tdTomato (Im. Shk.)
tdTomato (Training)
C
100 μm
AD
AV
DAPI DiI555
D
LFP recordings: AD inhibition during training
mCh
hM4Di-mCh
Theta
Gamma
Change in power (uV²/Hz)
Frequency (Hz)
Change in power (%)
E
100 μm
RSC
PreSub
DiI555
DAPI DiI555
F
AD→PreSub circuit coherence in vivo
Delta
Theta
Beta
Gamma
Change in coherence (%)
NS
Pre
Post
G
AD→RSC circuit coherence in vivo
H
Circuit-based cross-frequency coupling
Wild type
mCh
hM4Di-mCh
RSC amplitude (Hz)
AD phase (Hz)
MI
I
hM4Di labeling in PreSub and RSC
PreSub
RSC
CaMKII-hM4Di-mCh
J
CFC behavior - Training inhibition (PreSub)
Training
LTM test
Freezing (s)
K
CFC behavior - Training inhibition (RSC)
L
AD→RSC circuit, Training
eYFP
ChR2-eYFP
eArch-eYFP
M
Optogenetic mice in open field
Distance (cm)
eYFP control
AD→RSC eArch
AD→RSC ChR2
AD→PreSub eArch (C1ql2-Cre)
AD→RSC eArch (C1ql2-Cre)
AD→RSC →EC eArch
AV NpHR
AV→RSC NpHR

Figure S4. mEPSC and LFP Recordings from AD During CFC, and Chemogenetic Inhibition of PreSub or RSC Excitatory Neurons During CFC, Related to Figure 4

(A) AD mEPSC traces and cumulative (cum.) probability plots (16 home cage neurons, 18 CFC training neurons, n = 3 mice per group).

(B) Representative images of $cFos^+$ neurons in AD from the home cage group (Home), immediate shock group (Im. Shk.), and CFC training group (Training). Related to Figure 4D.

(C-D) DiI555 (red) electrode localization in AD, DAPI staining (blue) for LFP recordings from AD thalamus (C), AD inhibition using the chemogenetic strategy in Figure 4A during CFC training prevented the training-induced increases in theta and gamma rhythms (D) (n = 9 mCh mice, n = 7 hM4Di-mCh mice). Related to Figures 4E-4F.

(E) DiI555 (red) electrode localization in RSC and PreSub, DAPI staining (blue).

(F-G) AD→PreSub (F) and AD→RSC (G) circuit coherence Pre vs. Post CFC training (n = 7 mice per group).

(H) *In vivo* coupling between the theta rhythm phase in AD and gamma rhythm amplitude in RSC was enhanced by CFC training, which was blocked by AD inhibition during training (n = 7 mice per group). AD inhibition used the chemogenetic strategy in Figure 4A. Modulation index (MI).

(I-K) CaMKII-hM4Di-mCherry labeling in PreSub and RSC (I), C21-induced inhibition of excitatory neurons during CFC training in PreSub (J) or RSC (K) (n = 6 mCh mice, n = 8 hM4Di-mCh mice per brain region). LTM recall tests were performed 24 hr after training.

(L) Optogenetic AD→RSC circuit manipulation, CFC training data (n = 14 eYFP mice, n = 12 eArch-eYFP mice, n = 7 ChR2-eYFP mice). Surgery information is provided in the legend of Figure 4I.

(M) Various optogenetic groups of mice were used in a 10 min light-on open field session. eYFP, AD→RSC eArch, and AD→RSC ChR2 mice from Figure 4I, AD→PreSub eArch and AD→RSC eArch using C1ql2-Cre mice from Figure S5A, AD→RSC→EC eArch mice from Figure 4M, and AV NpHR and AV→RSC NpHR mice from Figure 5B.

Two-tailed unpaired t test (D, J-K), paired t test (F-G), and one-way ANOVA followed by Bonferroni post-hoc test (L-M). For statistical comparisons, $*p < 0.05$, $**p < 0.01$; NS, not significant.

Data are presented as mean ± SEM.

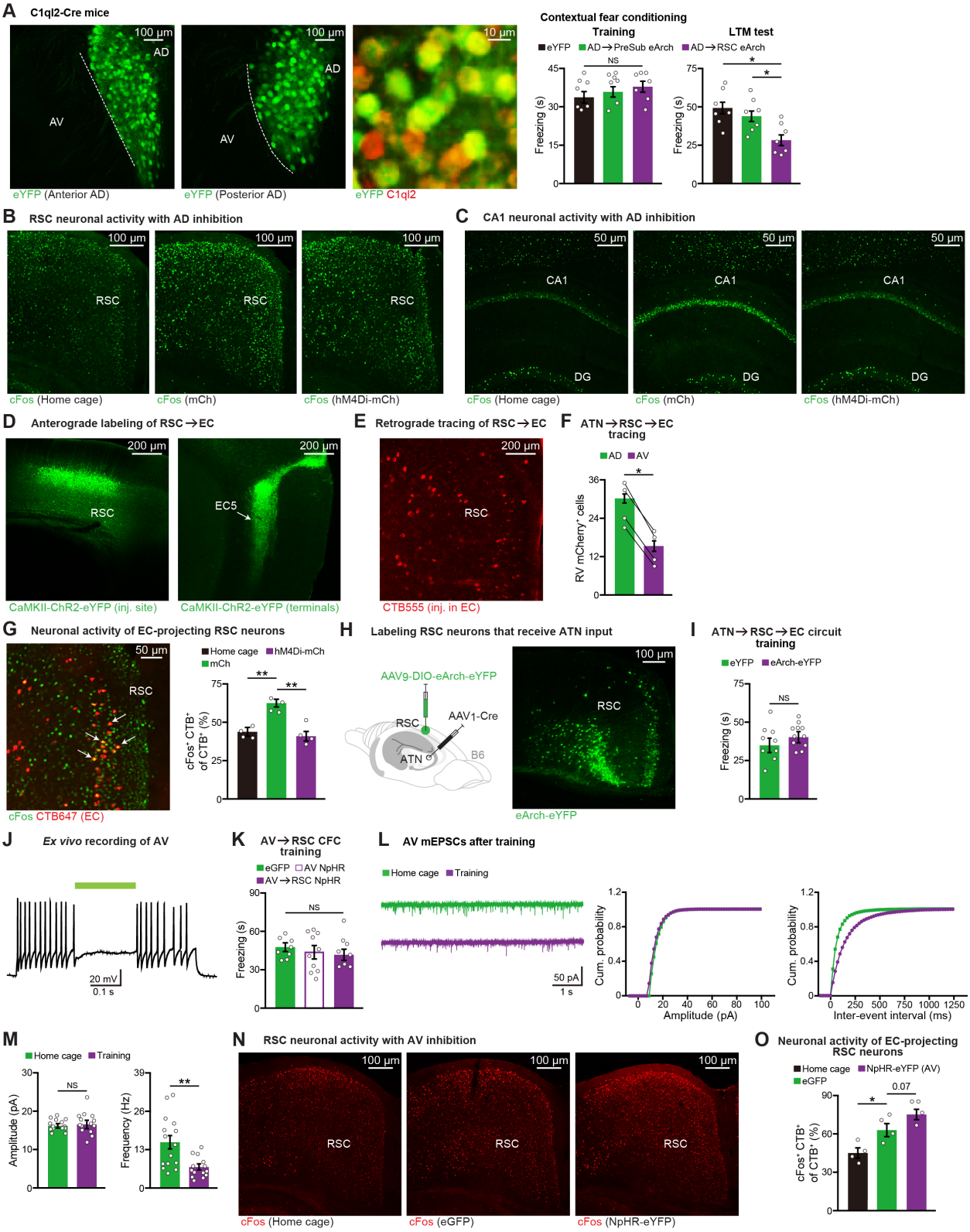
A
C1ql2-Cre mice
100 μm
AD
AV
eYFP (Anterior AD)
eYFP (Posterior AD)
10 μm
eYFP C1ql2
Contextual fear conditioning
Training
LTM test
eYFP
AD→PreSub eArch
AD→RSC eArch
NS
Freezing (s)
B
RSC neuronal activity with AD inhibition
RSC
cFos (Home cage)
cFos (mCh)
cFos (hM4Di-mCh)
C
CA1 neuronal activity with AD inhibition
50 μm
CA1
DG
D
Anterograde labeling of RSC→EC
200 μm
EC5
CaMKII-ChR2-eYFP (inj. site)
CaMKII-ChR2-eYFP (terminals)
E
Retrograde tracing of RSC→EC
CTB555 (inj. in EC)
F
ATN→RSC→EC tracing
AD
AV
RV mCherry+ cells
G
Neuronal activity of EC-projecting RSC neurons
Home cage
hM4Di-mCh
mCh
cFos+ CTB+ of CTB+ (%)
cFos CTB647 (EC)
H
Labeling RSC neurons that receive ATN input
AAV9-DIO-eArch-eYFP
AAV1-Cre
B6
ATN
eArch-eYFP
I
ATN→RSC→EC circuit training
eYFP
eArch-eYFP
J
Ex vivo recording of AV
20 mV
0.1 s
K
AV→RSC CFC training
eGFP
AV NpHR
AV→RSC NpHR
L
AV mEPSCs after training
Home cage
Training
50 pA
1 s
Cum. probability
Amplitude (pA)
Inter-event interval (ms)
M
Amplitude (pA)
Frequency (Hz)
N
RSC neuronal activity with AV inhibition
cFos (Home cage)
cFos (eGFP)
cFos (NpHR-eYFP)
O
Neuronal activity of EC-projecting RSC neurons
NpHR-eYFP (AV)
eGFP
0.07

Figure S5. AD Circuit Manipulations in C1ql2-Cre Mice, RSC→EC Circuit Tracing, and AV mEPSC Recordings After CFC Training, Related to Figures 4 and 5

(A) Injection of a Cre-dependent eYFP virus in the ATN region of C1ql2-Cre mice showing anterior and posterior AD labeling, and *eYFP*$^+$ neurons accounted for over 85% of the *C1QL2*$^+$ neurons (via antibody staining) in AD thalamus (n = 3 mice). Cre mice injected with a Cre-dependent eYFP control virus in the ATN region and two groups of Cre mice injected with a Cre-dependent eArch-eYFP virus in the ATN region along with optic fibers targeting bilateral PreSub or RSC were used in the CFC behavioral paradigm (n = 7 mice per group). Terminal inhibition was performed during CFC training, which was followed by a LTM recall test 24 hr later.

(B-C) Representative images of cFos$^+$ neurons in RSC (B) and hippocampal CA1 (C) from home cage, mCh, and hM4Di-mCh groups. Related to Figures 4J-4K.

(D-E) Anterograde labeling using CaMKII-ChR2-eYFP injected into RSC (D) and retrograde tracing by injecting CTB555 into EC (E) validated the RSC→EC circuit. EC layer 5 (EC5).

(F) Quantification of RV mCherry$^+$ cells in AD and AV from the ATN→RSC→EC tracing experiment in Figure 4L (n = 4 mice).

(G) *cFos* activation of EC-projecting RSC neurons labeled with CTB647 using home cage, training control (mCh), and training AD hM4Di groups (n = 4 mice per group). CTB647, red pseudocolor. Surgery information identical to Figure 4J with the addition of a CTB647 injection into EC.

(H-I) ATN→RSC→EC circuit manipulation experiment, RSC labeling (H), CFC training data (I) (n = 9 eYFP mice, n = 11 eArch-eYFP mice). Surgery information is provided in the legend of Figure 4M.

(J) Light-induced AV neuronal inhibition *ex vivo*.

(K) AV cell bodies or AV→RSC terminal manipulation experiment, CFC training data (eGFP n = 8 mice, AV NpHR n = 10 mice, AV→RSC NpHR n = 8 mice). Surgery information is provided in the legend of Figure 5A.

(L-M) AV mEPSC traces and cumulative (cum.) probability plots (L), AV mEPSC amplitude and frequency (M) (15 home cage neurons, 14 CFC training neurons, n = 3 mice per group).

(N) Representative images of *cFos*$^+$ neurons in RSC from home cage, eGFP, and NpHR-eYFP groups. Related to Figure 5C.

(O) *cFos* activation of EC-projecting RSC neurons labeled with CTB555 using home cage, training control (eGFP), training AV→RSC NpHR-eYFP groups (n = 4 mice per group). Surgery information for AV manipulation is provided in the legend of Figure 5C.

One-way ANOVA followed by Bonferroni post-hoc test (A, G, K, O), paired t test (F), and two-tailed unpaired t test (I, M). For statistical comparisons, *$p < 0.05$, **$p < 0.01$; NS, not significant.

Data are presented as mean ± SEM.

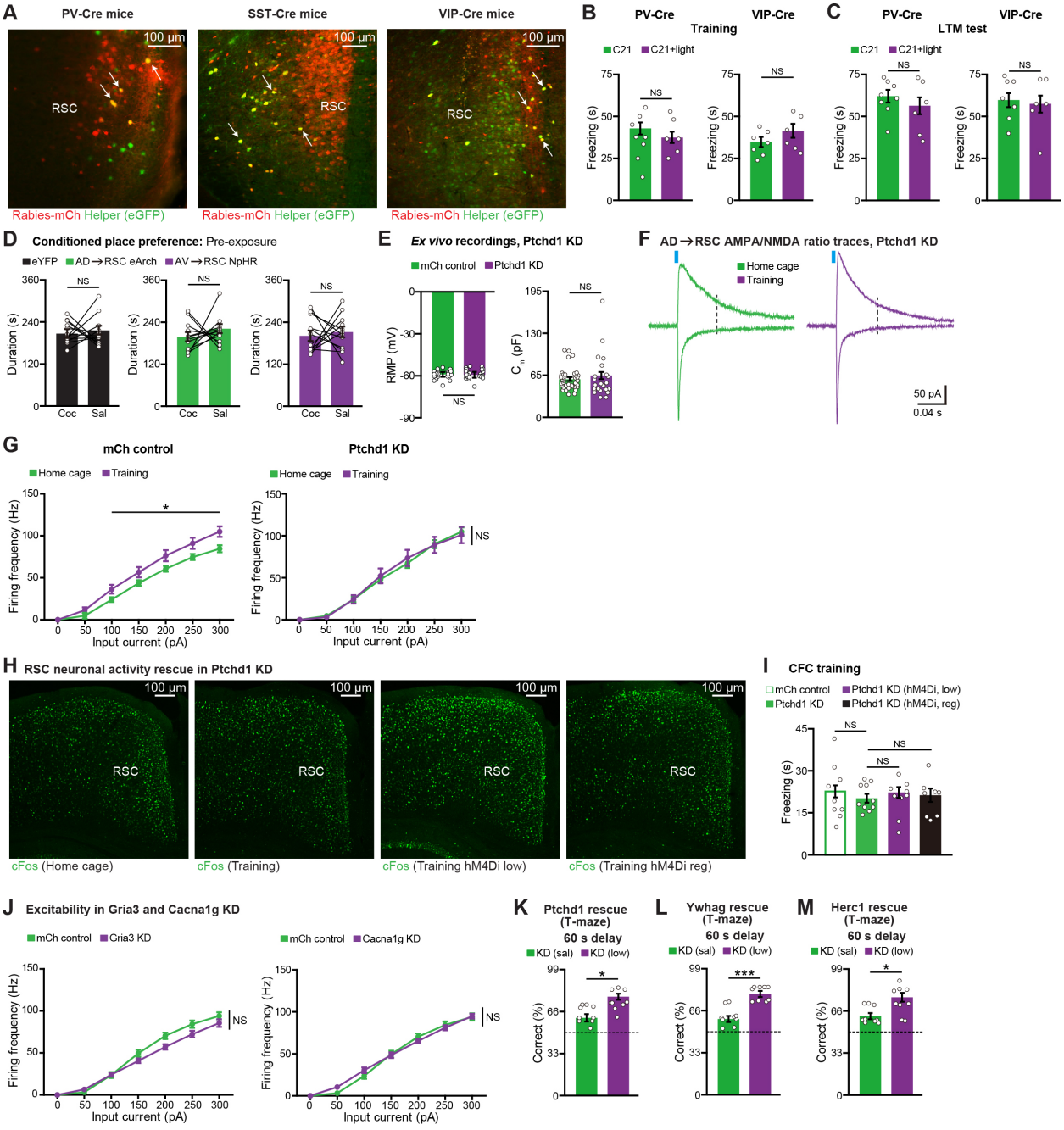

Figure S6. AV Inputs to Inhibitory Neuron Subtypes in RSC, and Electrophysiological Recordings in *PTCHD1*, *GRIA3*, and *CACNA1G* KD Mice, Related to Figures 5, 6, and 7

(A) Cre-dependent RV starter cells (yellow) in PV-Cre, SST-Cre, and VIP-Cre mice from RSC.

(B-C) AV→RSC inhibition with simultaneous *PV* or *VIP* activation in RSC during training from Figure 5I, CFC training data (B), LTM recall test (C) (PV-Cre: C21 n = 8 and C21+light n = 6 mice, VIP-Cre: C21 n = 7 and C21+light n = 6 mice). Surgery information is provided in the legend of Figure 5I.

(D) AD→RSC and AV→RSC terminal inhibition during training in the cocaine-induced conditioned place preference behavior test. Pre-exposure data plotted (n = 12 mice per group). Related to Figures 5K-5L.

(E) *Ex vivo* recordings from mCh control and *PTCHD1* KD AD neurons showing RMP and C_m (24 mCh neurons, 23 KD neurons, n = 3 mice per group). Surgery information is provided in the legend of Figure 1H.

(F) AD→RSC AMPA/NMDA ratio traces from *PTCHD1* KD experiment in Figure 6C.

(G) Neuronal excitability of AD neurons in home cage (before CFC training) and post-CFC training conditions, using mCh control and *PTCHD1* KD groups (mCh: 14 home cage and 13 training neurons, KD: 14 home cage and 16 training neurons, n = 3 mice per group).

(H) Representative images of $cFos^+$ neurons in RSC from home cage, training, training hM4Di low, and training hM4Di reg groups. Related to Figure 6G.

(I) CFC behavioral experiment using *PTCHD1* KD and rescue groups. Training data (mCh n = 9, KD n = 10 mice, KD low n = 9 mice, KD regular n = 8 mice). Related to Figure 6H.

(J) Neuronal excitability of AD neurons in mCh control, *GRIA3* KD, and *CACNA1G* KD groups (*GRIA3*: 15 mCh and 18 KD neurons, *CACNA1G*: 15 mCh and 14 KD neurons, n = 3 mice per group).

(K-M) KD rescue mice injected with saline (Sal group) or C21 low dose (Low group) prior to the spatial working memory T-maze test (60 s delay between sample and choice), for *PTCHD1* KD (K), *YWHAG* KD (L), and *HERC1* KD (M) (n = 9 mice per group). Surgeries used the strategy described in Figure 6D. Dashed line indicates chance level of performance (i.e., 50%).

Two-tailed unpaired t test (B-C, E, K-M), paired t test (D), two-way ANOVA with repeated measures followed by Bonferroni post-hoc test (G, J), and one-way ANOVA followed by Bonferroni post-hoc test (I). For statistical comparisons, *$p < 0.05$, ***$p < 0.001$; NS, not significant.

Data are presented as mean ± SEM.

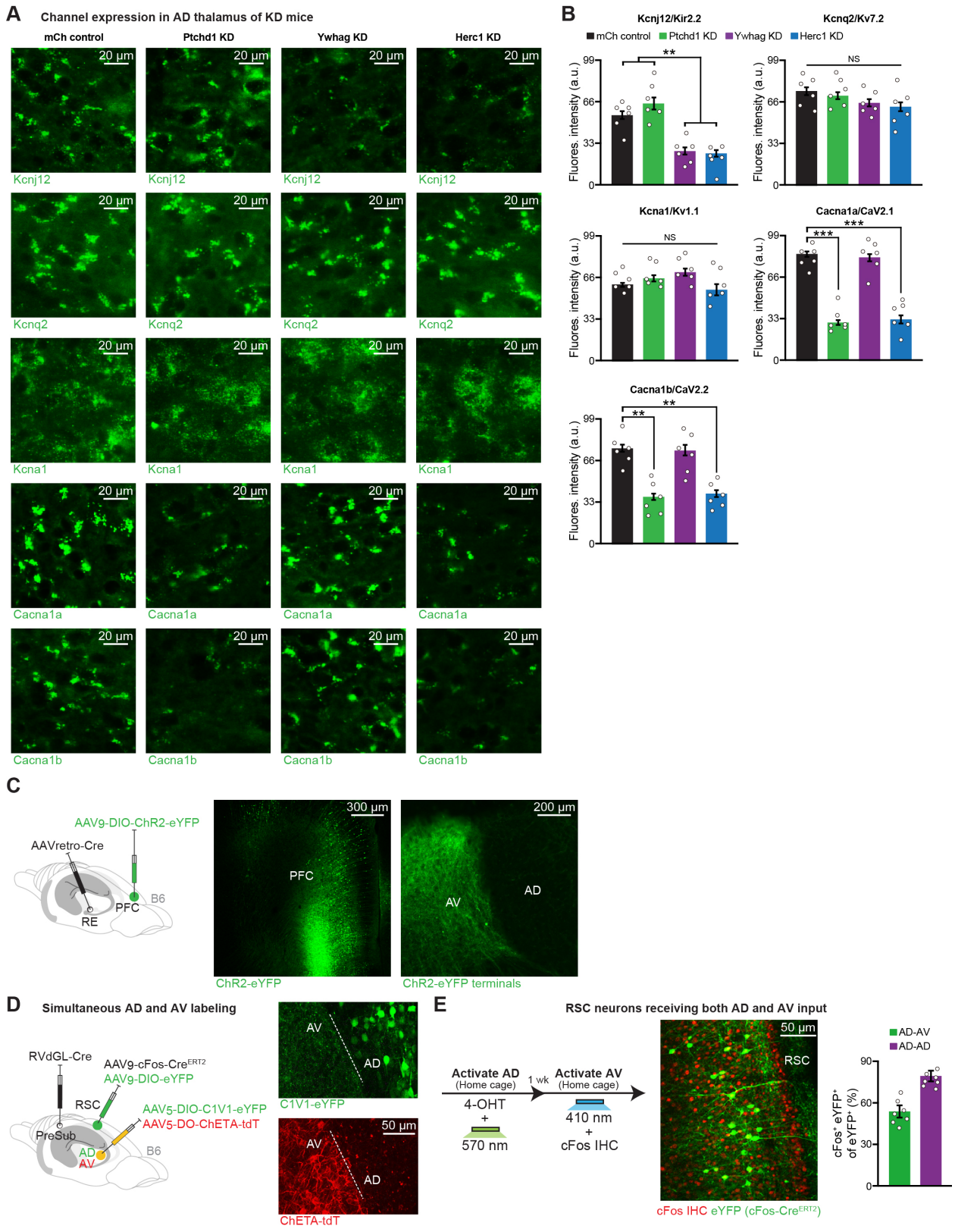
A
Channel expression in AD thalamus of KD mice
mCh control
Ptchd1 KD
Ywhag KD
Herc1 KD
20 μm
Kcnj12
Kcnq2
Kcna1
Cacna1a
Cacna1b
B
Kcnj12/Kir2.2
Kcnq2/Kv7.2
Kcna1/Kv1.1
Cacna1a/CaV2.1
Cacna1b/CaV2.2
mCh control
Ptchd1 KD
Ywhag KD
Herc1 KD
Fluores. intensity (a.u.)
99
66
33
0
**
NS
***
C
AAV9-DIO-ChR2-eYFP
AAVretro-Cre
PFC
B6
RE
300 μm
200 μm
AV
AD
ChR2-eYFP
ChR2-eYFP terminals
D
Simultaneous AD and AV labeling
RVdGL-Cre
AAV9-cFos-CreERT2
AAV9-DIO-eYFP
RSC
AAV5-DIO-C1V1-eYFP
AAV5-DO-ChETA-tdT
PreSub
AD
AV
B6
C1V1-eYFP
ChETA-tdT
50 μm
E
RSC neurons receiving both AD and AV input
Activate AD
(Home cage)
1 wk
Activate AV
(Home cage)
4-OHT
+
570 nm
410 nm
+
cFos IHC
50 μm
RSC
cFos IHC eYFP (cFos-CreERT2)
AD-AV
AD-AD
cFos+ eYFP+ of eYFP+ (%)
90
60
30
0

Figure S7. Channel Expression in KD AD Neurons, PFC Input to AV Thalamus, and RSC Neurons Receiving Both AD/AV Inputs, Related to Figure 7

(A-B) FISH staining in AD thalamus in mCh control, *PTCHD1* KD, *YWHAG* KD, and *HERC1* KD mice using probes for *Kcnj12*, *Kcnq2*, *Kcna1*, *Cacna1a*, and *Cacna1b* (A), quantification (B) (n = 6 mice per group). Fluorescence intensity (Fluores. intensity) is plotted in arbitrary units (a.u.).

(C) A retrograde Cre-expressing virus injected into nucleus reuniens (RE) with Cre-dependent ChR2-eYFP injected in PFC shows terminal labeling of RE-projecting PFC neurons in AV thalamus.

(D-E) Using retrograde RV expressing Cre from PreSub, AD neurons were labeled with Cre-On (DIO) C1V1-eYFP, AV neurons were labeled with Cre-Off (DO) ChETA-tdT, RSC active neurons were labeled using a cFos-Cre^{ERT2} virus (Ye et al., 2016) mixed with Cre-dependent eYFP. Dashed line indicates the border between AD and AV (D), AD terminals in RSC were activated using 570 nm light with simultaneous 4-OHT-induced tagging of *cFos*$^{+}$ RSC neurons in the home cage, one week later again in the home cage AV terminals in RSC were activated using 410 nm light followed by *cFos* staining for activated ensembles in RSC. Overlap between the 4-OHT-tagged RSC ensembles and *cFos* stained ensembles indicated that not all RSC neurons receive inputs from both AD and AV (i.e., ~25% receive input from AD or AV but not both). Sensitivity of this approach is demonstrated by high degree of overlap when both optogenetic proteins were expressed in AD (AD-AD) rather than one in AD and the other in AV (n = 7 mice per group). Immunohistochemistry (IHC) (E).

One-way ANOVA followed by Bonferroni post-hoc test (B). For statistical comparisons, $^{**}p < 0.01$, $^{***}p < 0.001$; NS, not significant.

Data are presented as mean ± SEM.